Seamless Grid Interaction for a Switched Doubly-fed Machine Propulsion Drive

Arijit Banerjee, Steven B. Leeb, and James L. Kirtley
Department of Electrical Engineering and Computer Science, Massachusetts Institute of Technology
Cambridge, Massachusetts, USA
arijit@mit.edu, sbleeb@mit.edu, kirtley@mit.edu

***Abstract*—Switched doubly-fed machine (DFM) drives can provide shaft speed control over a wide range without the need for a full power converter. Seamless shaft behavior across the complete speed range is achieved using a thyristor-based transfer switch in the stator of the DFM and appropriate control in the rotor converter. The drive must also operate without glitch with respect to the ac source. The seamless grid interaction is critical in applications such as in ship propulsion, where the drive may consume a major share of the generated power. This paper presents a coordinated control of the rotor converter that can ensure seamless operation for the switched-DFM drive with respect to the ac source. A laboratory setup emulating a ship microgrid is used to demonstrate the drive performance under different loading conditions.**

***Index Terms*—Doubly-fed machine, propulsion drive, wide speed range, microgrid, high power, front-end converter, coordinated control.**

I. Introduction

A switched doubly-fed machine (DFM) drive offers wide-speed range and four-quadrant operation with reduced power converter rating [1]. The drive is suitable for many high-power wide-speed-range applications, including ship propulsion. A typical switched-DFM drive operates over a speed range of ± 1.5 p.u (normalized relative to the ac source synchronous speed) with a rotor converter power rating of a third of the maximum shaft power. The reduction in the required converter rating directly translates into better drive efficiency, reduced filter size, lower fundamental drive frequency, and reduced harmonic content on both source and load side waveforms. In this drive, the rotor of the DFM is connected to an ac source using a back-to-back converter as shown in Fig. 1(a). The stator is connected to a thyristor-based transfer switch that can toggle the stator connection between two different configurations [2]. In the low-speed induction topology (LSI) of the switched-DFM drive, the stator is shorted during low-speed operation and is connected to the ac source during high-speed operation [3]. In the low-speed synchronous topology (LSS) of the switched-DFM drive, the stator is connected to a dc source at low speed and is connected to the ac source at high speed [4]. In general, for both the topologies, the entire shaft power is provided by the rotor in the low-speed operating mode and is shared by the stator and the rotor in the high-speed operating mode. Both the topologies have comparative advantages and limitations that make one preferable over the other based on the DFM design, steady-state consideration

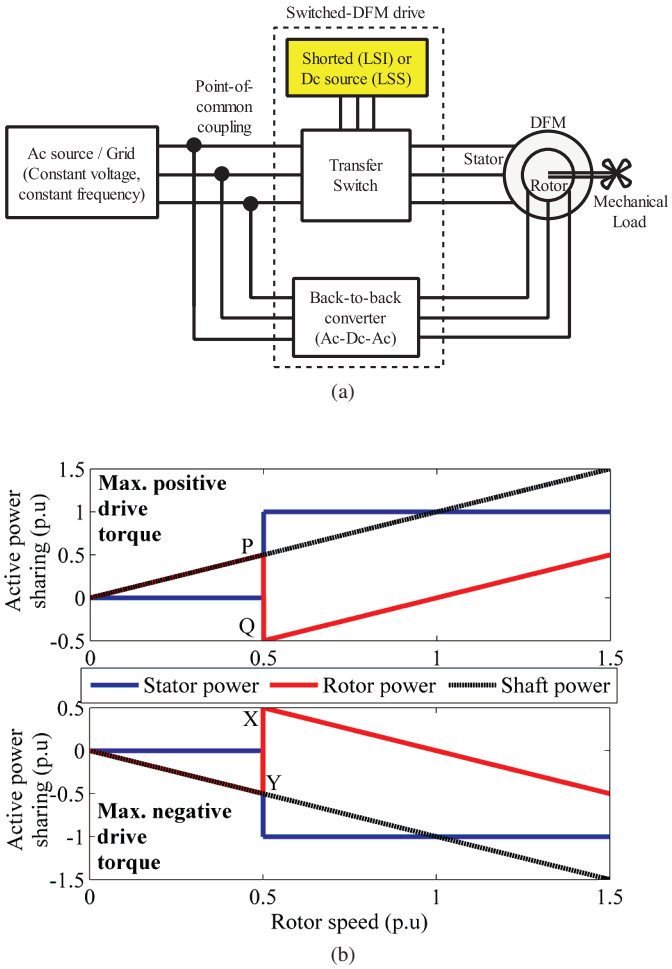

Figure 1. (a) A general architecture of a switched-DFM drive (b) Sharing of the shaft power by an ideal switched DFM drive.

[5], transient performances [6], and the application-specific requirements.

The switched-DFM drive has been shown to operate with seamless shaft behavior in and through the low-speed and high-speed modes with appropriate control on the rotor drive-end converter and mode transition instant of the stator transfer switch [7]. However, the drive must also interact with the ac source seamlessly irrespective of the operating modes. This is critical for the stability of the ac grid as well as for the

978-1-4799-7941-7/15/$31.00 ©2015 IEEE

intermediate dc-link between the front-end and the drive-end converters. Assuming an ideal DFM (with no resistive losses and leakages) producing a rated drive torque of 1 p.u, the active power required in the stator during the low-speed operation is zero and the shaft power equals the rotor power as shown in Fig. 1(b). At the transition instant (denoted by P in Fig. 1(b)) from the low-speed to the high-speed mode, the active power in the stator of the DFM changes from zero to 1 p.u. Instantaneously, the rotor back-to-back converter withdraws power from the rotor to ensure a mechanically "bumpless" transition at the shaft. The power withdrawn from the rotor must be seamlessly transferred to the point of common-coupling (PCC) in Fig.1(a) such that the active power drawn from the ac source is "bumpless" as well. A converse scenario appears with respect to the power consumption from the ac source during the braking of the drive with a torque of -1 p.u as shown in Fig. 1(b).

A stiff ac source with a sufficient active power reserve can sustain a sudden change in power demand if the active power balance at the PCC is not met during mode transition. The seamless grid interaction at the PCC becomes more critical in applications where the switched-DFM drive may consume a major share of the generated ac power or in cases where a large inductive line exists between the PCC and the ac source. For example, in an islanded ship microgrid, the propulsion drive may consume as much as ninety percent of the ship ac generator capability [8]. In this case, a large swing in power requirement can destabilize the ac grid. Similar arguments are valid for the reactive power requirement of the switched-DFM drive in the two modes of operation and during the mode transition.

The stability of the intermediate dc link must also be ensured during the different modes of the drive as well as during the mode transition. At the instance of mode transition, the power supplied by the rotor of the switched DFM instantly reverses polarity as can be seen in Fig. 1(b). This calls for an instant change in the direction of active power flow in the dc link. The front-end converter control must ensure a seamless bidirectional power flow to ensure stability of the dc link [9], [10].

This paper presents a coordinated control of the front-end and the drive-end converter of a switched-DFM drive to ensure a seamless drive operation relative to the ac source, dc link and the mechanical shaft. The paper illustrates an emulated laboratory ship microgrid that is configured both to generate power through parallel operation of two synchronous generators, and to also consume 80% of the generated power through a switched DFM drive connected to a propulsion load. Experimental results are presented to verify stable operation of the ac source and the intermediate dc-link during the different modes of the drive operation.

II. Grid Interaction of a Switched-DFM drive

The switched-DFM drive interacts with the ac grid through the rotor under all operating modes and through the stator only during the high-speed mode. The two degrees of freedom of the front-end converter are used to maintain the intermediate dc-link voltage and provide additional reactive power support to the grid, if necessary. This section highlights the sizing and control of the front-end converter to ensure a seamless grid interaction of the overall drive under different operating conditions.

A. Front-end converter sizing analysis

Denoting V_b (peak per-phase) to be the required maximum rotor voltage referred to the stator, N_M to be the rotor-to-stator winding turns-ratio of the DFM, and assuming that the drive-end converter operates as a two-level voltage source converter operating with conventional space-vector modulation, the required nominal dc link voltage, $V_{dc,nom}$ to operate the drive over the full speed range is given by,

$$V_{dc,nom} = \sqrt{3} V_b N_M G_{dc} \tag{1}$$

where G_{dc} is an extra margin provided to the dc-link voltage and is typically of the order of $1.04 - 1.1$. More often than not, a grid-side transformer interfaces between the front-end converter and the ac source. Denoting the nominal duty ratio of the front-end converter to be $D_{FE,nom}$, the nominal grid voltage magnitude to be $V_{g,nom}$ (peak per-phase), and assuming that the front-end converter is also a two-level voltage source converter operating with conventional space-vector modulation, the required turns-ratio of the grid side transformer (N_T) for proper grid interfacing is given by,

$$N_T = \frac{D_{FE,nom} V_b N_M G_{dc}}{V_{g,nom}} \tag{2}$$

For an active power P_r to be supplied to the DFM rotor from the drive-end converter, the required dc link current is:

$$\begin{array}{ll} I_{dc} = \frac{P_r}{\eta_{de} V_{dc,nom}} & for\ P_r > 0 \\ I_{dc} = \frac{\eta_{de} P_r}{V_{dc,nom}} & for\ P_r < 0 \end{array} \tag{3}$$

and the required current to be drawn from the ac grid by the front-end converter is:

$$\begin{array}{ll} I_f = \frac{2}{3} \frac{P_r}{\eta_{fe} \eta_{de} N_T V_{g,nom}} & for\ P_r > 0 \\ I_f = \frac{2}{3} \frac{\eta_{fe} \eta_{de} P_r}{N_T V_{g,nom}} & for\ P_r < 0 \end{array} \tag{4}$$

where η_{de} and η_{fe} are the efficiencies of the drive-end and the front-end converters respectively. Additionally, the front-end converter may be designed to handle a part of the DFM magnetizing current or provide additional grid-side reactive power support based on the DFM design or the application requirement.

Assuming constant dc-link and ac grid voltages, the dc-link current and the front-end converter current injected to the ac grid are a scaled version of the rotor active power. In conclusion, the front-end converter voltage rating is governed by the required dc link voltage for the drive to operate over the full speed range. In addition, the current rating is governed by the required rotor power and the additional reactive power support, if necessary.

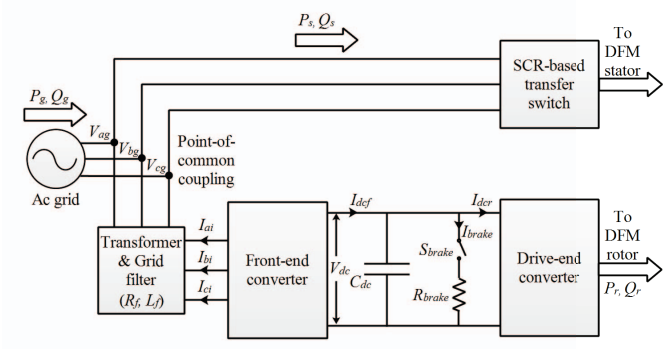

Figure 2. Power flow and grid interaction of the switched DFM drive.

B. Front-end converter control

The front-end converter interfaces the ac grid through a filter and the grid-side transformer as shown in Fig. 2. The filter and the grid-side transformer can be modeled as a lumped series resistance R_f and an inductance L_f for control purposes. In the d-q reference frame, with the d-axis aligned with the ac source voltage vector, the system equations governing the power flow between the ac-grid and the front-end converter are given by:

$$V_{fd} = L_f \frac{dI_{fd}}{dt} + R_f I_{fd} - \omega_g L_f I_{fq} - V_g \tag{5}$$

$$V_{fq} = L_f \frac{dI_{fq}}{dt} + R_f I_{fq} + \omega_g L_f I_{fd} \tag{6}$$

where V_g is the ac-grid voltage magnitude (peak per-phase), ω_g is the ac-grid frequency, (V_{fd}, V_{fq}) are the d-axis and q-axis voltages, respectively, that are commanded by the front-end converter, and (I_{fd}, I_{fq}) are the d-axis and q-axis currents, respectively, fed by the front-end converter to the grid. The required reference frame angle θ_g for the d-q transformation of the measured grid phase voltages (V_{ag}, V_{bg}, and V_{cg}) and the inverter currents (I_{ai}, I_{bi}, and I_{ci}) is obtained from a three-phase phase-locked loop (PLL) designed to track the grid voltage and frequency [11] as shown in the control architecture for the front-end converter in Fig. 3.

The inner-loop proportional-integral (PI) current controllers are designed based on (5) and (6) with appropriate feedforward terms to eliminate the effect of the cross-coupling terms due to L_f and the grid-voltage magnitude. The reference command to the inner loop d-axis current controller is set by the outer loop dc-link voltage controller. The q-axis current controller is commanded based on the required reactive power support from the front-end converter. The coordination between the front-end and the drive-end converters is taken into consideration during the design of the outer loop controllers to ensure a seamless mode transition of the switched-DFM drive relative to the ac-grid.

The dc-link voltage V_{dc} is set by the net charging current to the dc-link capacitor C_{dc}, which is the difference between the current drawn from the front-end converter I_{dcf}, the current delivered to the drive-end converter I_{dcr}, and the current in the braking resistor I_{brake} as shown in Fig. 2. The dynamical equation governing the dc-link voltage is given by,

$$C_{dc} \frac{dV_{dc}}{dt} = I_{dcf} - I_{dcr} - I_{brake} \tag{7}$$

Neglecting switching ripple, the active power P_r drawn by the rotor of the DFM from the dc link can be related to the drive-end converter current I_{dcr} by,

$$\begin{aligned} P_r &= \eta_{de} V_{dc} I_{rdc} \quad for\ P_r > 0 \\ P_r &= \tfrac{1}{\eta_{de}} V_{dc} I_{rdc} \quad for\ P_r < 0 \end{aligned} \tag{8}$$

Defining S_{brake} as the switching function of the braking resistor R_{brake} connected to the dc link, the current in the braking resistor is given by,

$$I_{brake} = S_{brake} \frac{V_{dc}}{R_{brake}} \tag{9}$$

Therefore, the current I_{dcr} and I_{brake} in (7) can be substituted using (8) and (9) as:

$$\begin{aligned} I_{dcf} &= C_{dc} \tfrac{dV_{dc}}{dt} + \underbrace{\left(\frac{P_r}{\eta_{de} V_{dc}}\right) + S_{brake} \frac{V_{dc}}{R_{brake}}}_{feedforward\ terms} \quad for\ P_r > 0 \\ I_{dcf} &= C_{dc} \tfrac{dV_{dc}}{dt} + \underbrace{\left(\frac{\eta_{de} P_r}{V_{dc}}\right) + S_{brake} \frac{V_{dc}}{R_{brake}}}_{feedforward\ terms} \quad for\ P_r < 0 \end{aligned} \tag{10}$$

The dc-link voltage controller is designed using (10) with appropriate feedforward terms that command the required the front-end converter current I^*_{dcf}. The feedforward terms include the active power supplied to the rotor of the DFM by the drive-end converter and the switching function of the braking resistor. The feedforward terms help in minimizing the delay in dc-link power balance in case a step perturbation in active power requirement is demanded by the switched-DFM drive during the mode transition. Similar control strategies have been widely used in the literature for generic ac-to-dc converter control [12], [13], [14].

The relationship between the output of the dc-link voltage controller I^*_{dcf} and the reference d-axis converter current I^*_{fd} can be established through the active power balance across the front-end converter and is given by,

$$\begin{aligned} V_{dc} I^*_{dcf} &= -\tfrac{3}{2} \eta_{fe} V_g I^*_{fd} \quad for\ I^*_{dcf} > 0 \\ V_{dc} I^*_{dcf} &= -\tfrac{3}{2} \tfrac{1}{\eta_{fe}} V_g I^*_{fd} \quad for\ I^*_{dcf} < 0 \end{aligned} \tag{11}$$

The negative sign appears due to the assumed direction of the front-end converter current. For simplicity, the conditional gains and feedforward terms that depend on the direction of the power flow are not explicitly shown in the control architecture in Fig. 3.

In a ship or a locomotive microgrid, with the propulsion load power taking the major share of the total power generation capability, a complete regenerative braking using the front-end converter may destabilize the ac grid. It is necessary to

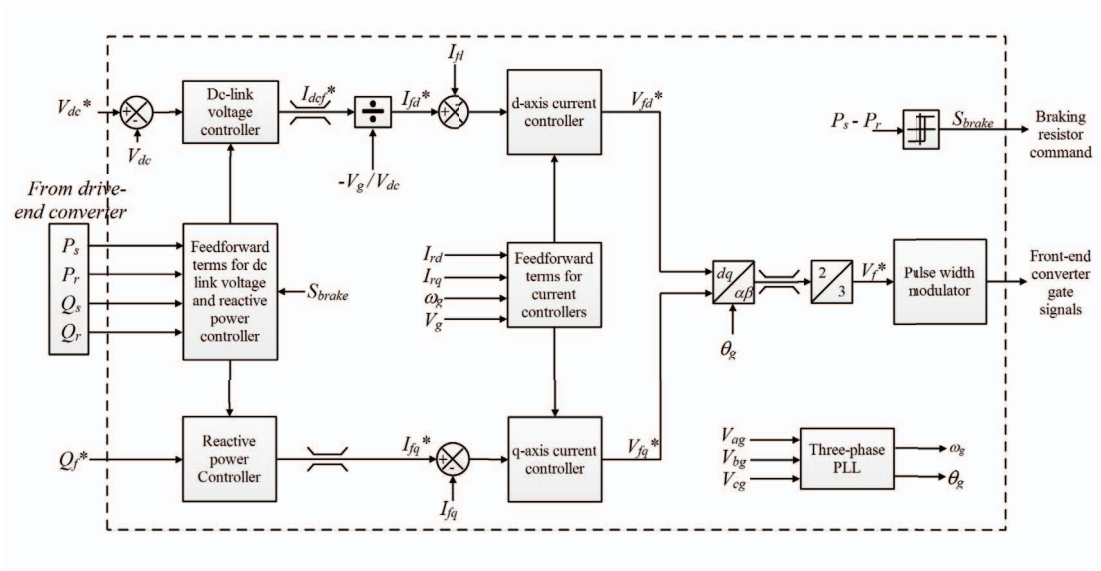

Figure 3. Control architecture of the front-end converter of the switched-DFM drive for seamless grid interaction under all operating modes.

share the power recovered from the mechanical drive train between passive dissipation in the braking resistor and the active regeneration to the ac grid during the braking operation of the drive. The braking resistors are sized such that the power regenerated to the ac grid is within the allowable grid-frequency stability limits.

The braking resistors can be turned ON ($S_{brake} = 1$) or OFF ($S_{brake} = 0$) based on the relative magnitude of the measured dc link voltage and a maximum allowable dc-link voltage threshold. However, this may lead to unnecessary turn-on of the braking resistor during the low-speed to high-speed mode transition as the power flow to the dc link reverses instantaneously. Using an alternative approach, the braking resistor is operated based on the active power balance in the DFM. The total active power delivered to the DFM is the sum of the stator and the rotor active powers under all operating conditions. A low-speed to high speed mode transition can be differentiated from a braking operation by the sign of the total active power delivered to the DFM. This is used to command the switching signal of the braking resistor as

$$\begin{aligned} S_{brake} &= 1 \quad for\ P_s + P_r < P_L \\ S_{brake} &= 0 \quad for\ P_s + P_r > P_H \end{aligned} \tag{12}$$

where P_L and P_H are the negative active power bounds for a hysteresis comparator. The active power bounds are designed based on the allowable regenerative braking to the ac grid and the size of the braking resistor.

III. Setup Description

The schematic of the laboratory setup used to evaluate the overall operation and the grid interaction of a switched DFM drive is shown in Fig. 4. Two dc motor-driven synchronous generators operating in parallel make the ac grid of 146 V (line-to-line, rms), 40 Hz. The choice of the ac grid frequency ensures that the off-the-shelf DFM with the parameters given in Table I remains within the rated operating speed of 1800 rpm. Correspondingly, the ac source voltage is adjusted to ensure that the DFM operates with a rated stator flux in ac grid-connected mode. The total active power generation capability by the two generators is 1.4 kW. The switched-DFM drive consumes 80% of the total generated power at full-load condition. The generators are loaded with a 20% base resistive load that emulates the auxiliary load of a ship. The rotor of the DFM is connected to the back-to-back converters that can produce a variable voltage variable frequency ac waveform at the rotor terminal from the fixed frequency ac grid. Two Texas Instruments High Voltage Motor Control & PFC Developer's Kits make the front-end and the drive-end converters. A grid-side auto-transformer and a three-phase LCL filter interface between the ac grid and the front-end converter.

The stator of the DFM is connected to the SCR-based transfer switch that can toggle the stator connection based on the operating drive speed. The phase sequence change over relay ensures that the drive can operate over ±1800 rpm with the same rotor power converter rating. At low-speed mode, the stator can be connected to a separate 20 V dc source in the LSS topology or shorted together in the LSI topology using the switch S_{ind}. The shaft of the DFM is loaded by a permanent magnet synchronous generator (PMSG), which is connected to a dc-electronic load bank. The diode bridge placed between the load bank and the PMSG ensures unidirectional current flow irrespective of the direction of shaft rotation. The following sections describe the control for each subsystem of the setup.

A. Control of the ac source: Parallel operation of the synchronous generators

The salient-pole wound-field synchronous generators are driven by two separate dc motors that are individually powered from two controllable dc power supplies. The output voltage of

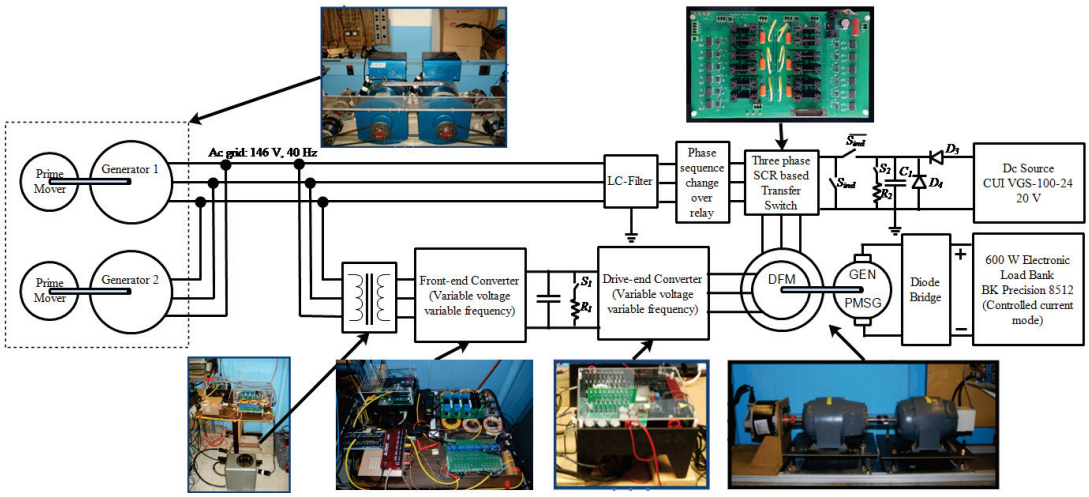

Figure 4. Experimental setup to validate the overall performance and the grid interaction of a switched-DFM drive. The setup emulates a ship power system with 80% share for the propulsion load and the remaining 20% share for the auxiliary loads of the total generated power.

the controllable dc power supply is equivalent to the throttle input for a mechanical prime-mover. The field windings of the synchronous generators are individually excited from two additional controllable dc power supplies. The generator speed, terminal voltage, and the armature currents are measured and used as feedback signals by the generator controller. The control algorithm runs at 960 Hz. Two proportional-integral (PI) controllers, with droop for active power sharing, command the voltage of the dc motors emulating a typical prime-mover control for a synchronous generator. Two additional PI controllers, with feedback for reactive power sharing, command the dc power supplies that energize the field windings of the generators based on the measured terminal voltage.

B. Control of the switched-DFM drive: Coordinated control of the drive-end converter, front-end converter and the SCR-based transfer switch

The control of the switched DFM drive is achieved by programming the control architectures of the front-end converter and the drive-end converter [7] in two Piccolo microcontrollers - TMS320F28035 that individually have a 32-Bit CPU, 12-bit ADCs, and a 60 MHz clock. The two controllers communicate based on the requirement of the feedforward terms by the front-end converter. The SCR-based transfer switch is commanded at an appropriate transition instant from the drive-end converter.

The results presented in this paper correspond to the LSS topology of the switched-DFM drive. The mode transition speed is set at 775 rpm with a hysteresis band of ± 18 rpm i.e. the stator is connected to the ac grid when the drive speed exceeds 793 rpm (denoted by ω_1). Alternatively, the stator is connected to the dc source when the drive speed falls below 757 rpm (denoted by ω_2). The drive is designed to provide 70% of the rated torque capability during low-speed mode. The nominal dc-link voltage is designed at 100 V with adequate margin to overcome the device drops and is maintained by the front-end converter. The transformer turns-ratio is set at 0.4 for proper grid interfacing of the front-end converter. The front-end converter operates with a nominal duty ratio of 0.8.

C. Control of the load: Current control of the dc electronic load bank

The PMSG coupled to the DFM is connected to the dc electronic load bank (BK Precision 8512), which is operated in constant current mode. The load bank is commanded with a current value every 120 ms by a controller programmed in NI-Labview through serial communication. The controller measures the speed of the DFM rotor and can generate various load torque-speed characteristic. Apart from loading the DFM with a quadratic load torque profile, typical for a ship propulsion, other load perturbations can also be enforced at the DFM shaft.

IV. Experimental Results

The reference speed of the DFM is commanded with a step function as shown in Fig. 5(a). The seamless operation of the DFM drive across the complete speed range with bumpless torque at the shaft is shown in Fig. 5(a). The active power shared between the stator and the rotor is shown in Fig. 5(b). At the instant of low-speed to high-speed mode transition (denoted by A in Fig. 5(b)), the stator active power undergoes a step increase while instantaneously the rotor active power polarity reverses to ensure a minimum perturbation at the shaft torque/speed. At this instant, the dc-link current polarity also reverses. The dc-link voltage is maintained within 3% of the nominal value as shown in Fig.5(c). The ac-grid voltage and frequency decrease as the loading on the generator increases and vice versa due to the programmed droop in the generator controller as shown in Fig. 5(d). The ac-grid voltage and frequency remain within $\pm 6\%$ of the nominal values as the drive goes through the different operating regimes during acceleration and braking. The sharing of active power between

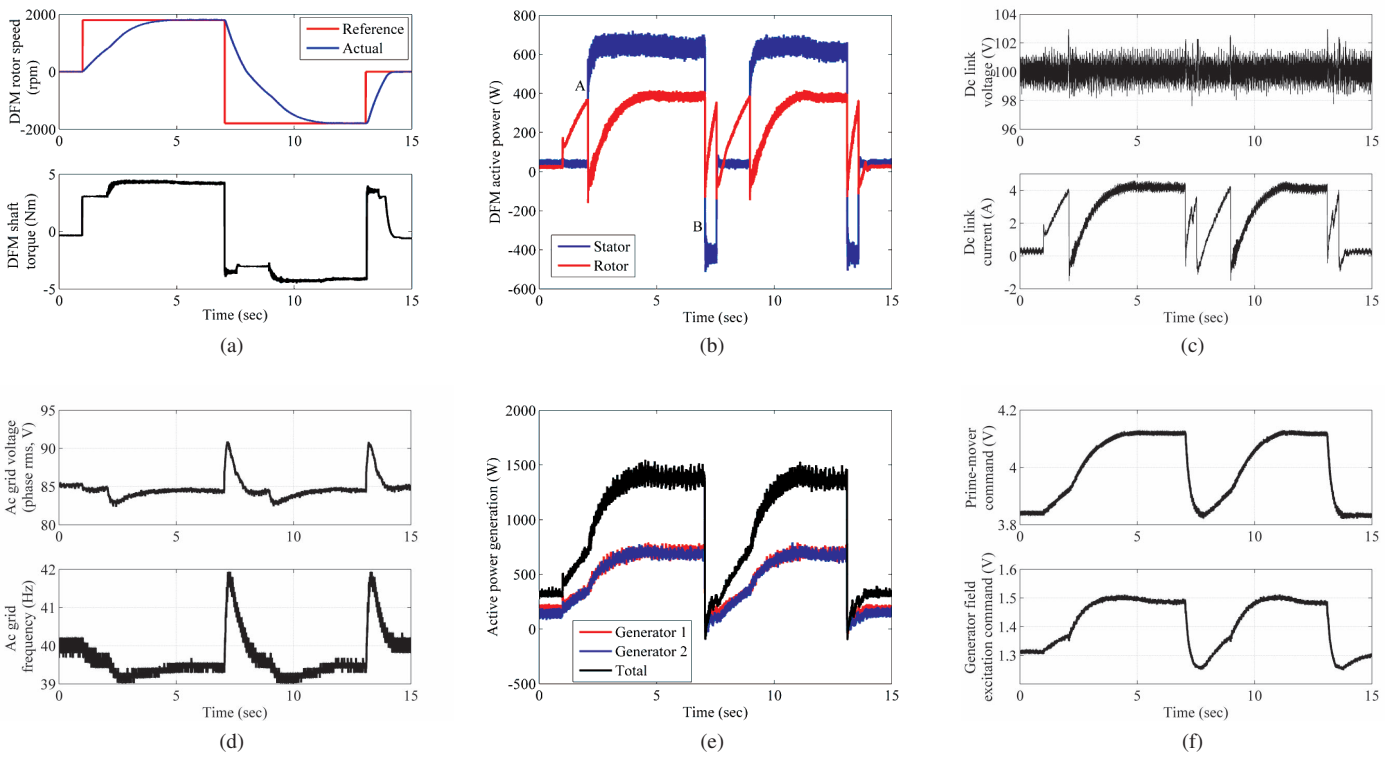

Figure 5. Experimental results for a step command in reference speed with the switched DFM drive operating within the full speed range. (a) DFM rotor speed and the drive torque (b) Sharing of the active power between the stator and the rotor of the DFM (c) Dc-link voltage and the dc-link current (d) Ac-grid voltage magnitude and frequency (e) Sharing of the generated active power between the two synchronous generators (f) Voltage command to the dc motor and the field winding of one of the synchronous generators.

the two synchronous generators is achieved under all loading conditions as seen in Fig. 5(e). The coordinated control of the back-to-back converters ensures that the ac generators do not perceive any sudden disturbance in active power at the mode transition instants. The generators are loaded with a base load of 350 W using a resistive load to prevent reverse power flow during the braking operation of the drive (denoted by B in Fig. 5(b)). The voltage command to the dc motor driving one of the synchronous generators along with the voltage command to the generator field winding is plotted in Fig. 5(f). Both of these commands have a much lower bandwidth but operate seamlessly irrespective of the DFM operating mode. Similar behavior is observed in all the values during the negative speed range operation of the drive.

The DFM drive is next subjected to an alternating speed reference command between 680 rpm and 860 rpm with a frequency of 1 Hz. The drive operates alternatively in the low-speed mode (marked by B) and the high-speed mode (marked by A) as shown in Fig. 6. The coordinated control of the switched DFM drive ensures that the dc-link voltage, ac-grid voltage, and the ac-grid frequency are not only stable but also maintained within small variations.

The DFM drive is next commanded with a constant reference speed of 775 rpm. The dc electronic load bank is programmed to alternate the loading on the shaft between 20% and 60% of the full load torque with a frequency of 1 Hz. As the load torque is turned on and off, the speed perturbation at the shaft causes the DFM drive to alternate between the low-speed mode (marked by B) and the high-speed mode (marked by A). The dc-link voltage, ac grid voltage, and ac grid frequency are once again stable and maintained within small variations during the load disturbances as shown in Fig. 7.

Table I
EXAMPLE DFM PARAMETERS: 1 HP, 220-V/150-V, 4-POLE, 60-HZ, 3.6-A/4-A

Parameters	Actual	Normalized
Stator resistance	3.575 Ω	0.1013
Rotor resistance (ref. to stator)	4.229 Ω	0.1199
Stator leakage inductance	9.6 mH	0.1024
Rotor leakage inductance (ref. to stator)	9.6 mH	0.1024
Mutual inductance	165 mH	1.763
Stator current rating	5.09 A (peak)	1
Rotor current rating (ref. to stator) (I_r)	3.857 A (peak)	0.7576

V. CONCLUSIONS

The paper presented a coordinated control of the front-end converter and the drive-end converter for a switched-DFM drive. This is necessary to ensure a bumpless operation of the switched-DFM drive not only relative to the machine shaft torque/speed, but also relative to the ac source. The seamless performance of the switched-DFM drive can result

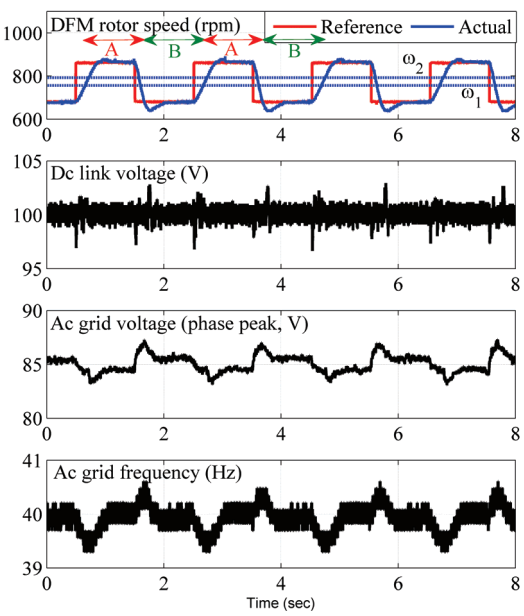

Figure 6. Experimental results: Variation in the dc-link voltage, ac-grid voltage, and the ac-grid frequency with alternate reference speed for the DFM around the mode transition speed. A: High-speed mode (the stator is connected to the ac grid) B: Low-speed mode (the stator is connected to the dc source)

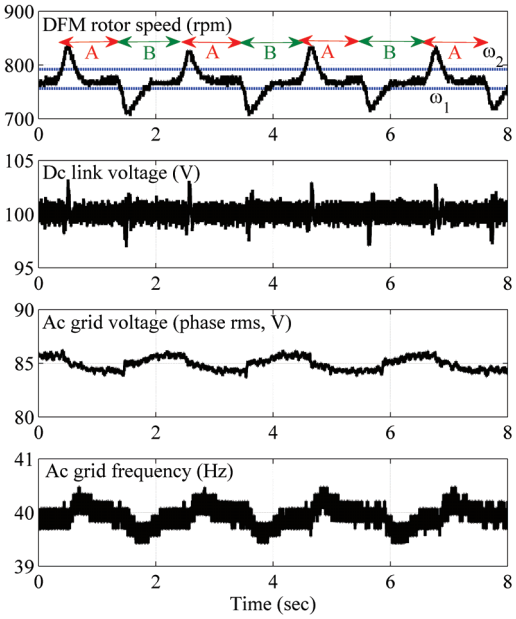

Figure 7. Experimental results: Variation in the dc-link voltage, ac-grid voltage, and the ac-grid frequency with an oscillating load disturbance at the DFM shaft. The DFM operates in the low-speed and the high-speed mode alternatively. A: High-speed mode (the stator is connected to the ac grid) B: Low-speed mode (the stator is connected to the dc source).

in a compact and efficient drive with reduced power converter size thus enabling operation over a wide speed range.

ACKNOWLEDGMENT

This research was performed with support from the Kuwait Foundation for the Advancement of Sciences (KFAS) through the Kuwait-MIT Center for Natural Resources and the Environment (CNRE), the Skoltech-MIT SDP Program, and The Grainger Foundation.

REFERENCES

[1] A. Banerjee, M. Tomovich, S. Leeb, and J. Kirtley, "Power converter sizing for a switched doubly fed machine propulsion drive," *Industry Applications, IEEE Transactions on*, vol. 51, no. 1, pp. 248–258, Jan 2015.

[2] A. Banerjee, A. Chang, K. Surakitbovorn, S. Leeb, and J. Kirtley, "Bumpless automatic transfer for a switched doubly-fed machine propulsion drive," *Industry Applications, IEEE Transactions on*, vol. PP, no. 99, pp. 1–1, 2015.

[3] L. Morel, H. Godfroid, A. Mirzaian, and J.-M. Kauffmann, "Double-fed induction machine: converter optimisation and field oriented control without position sensor," *Electric Power Applications, IEE Proceedings* -, vol. 145, no. 4, pp. 360–368, Jul 1998.

[4] S. B. e. Leeb, "How much dc power is necessary?" *Naval Engineers Journal*, vol. 122, no. 2, pp. 79–92, 2010.

[5] A. Banerjee, S. B. Leeb, and J. L. Kirtley, "A comparison of switched doubly-fed machine drive topologies for high power applications," *International Electrical Machines and Drive Conference , IEEE*, p. to appear, May 2015.

[6] ——, "Transient performance comparison of switched doubly-fed machine propulsion drives," *Transportation Electrification Conference and Expo , IEEE*, p. to appear, Jun 2015.

[7] A. Banerjee, M. Tomovich, S. Leeb, and J. Kirtley, "Control architecture for a switched doubly fed machine propulsion drive," *Industry Applications, IEEE Transactions on*, vol. 51, no. 2, pp. 1538–1550, March 2015.

[8] M. Steurer, M. Andrus, J. Langston, L. Qi, S. Suryanarayanan, S. Woodruff, and P. Ribeiro, "Investigating the impact of pulsed power charging demands on shipboard power quality," in *Electric Ship Technologies Symposium, 2007. ESTS '07. IEEE*, May 2007, pp. 315–321.

[9] P. Verdelho and G. Marques, "Dc voltage control and stability analysis of pwm-voltage-type reversible rectifiers," *Industrial Electronics, IEEE Transactions on*, vol. 45, no. 2, pp. 263–273, Apr 1998.

[10] J. Espinoza, G. Joos, M. Perez, and T. Moran, "Stability issues in three-phase pwm current/voltage source rectifiers in the regeneration mode," in *Industrial Electronics, 2000. ISIE 2000. Proceedings of the 2000 IEEE International Symposium on*, vol. 2, 2000, pp. 453–458 vol.2.

[11] S.-K. Chung, "A phase tracking system for three phase utility interface inverters," *Power Electronics, IEEE Transactions on*, vol. 15, no. 3, pp. 431–438, May 2000.

[12] D.-C. Lee, G.-M. Lee, and K.-D. Lee, "Dc-bus voltage control of three-phase ac/dc pwm converters using feedback linearization," *Industry Applications, IEEE Transactions on*, vol. 36, no. 3, pp. 826–833, May 2000.

[13] J. Jung, S. Lim, and K. Nam, "A feedback linearizing control scheme for a pwm converter-inverter having a very small dc-link capacitor," *Industry Applications, IEEE Transactions on*, vol. 35, no. 5, pp. 1124–1131, Sep 1999.

[14] D.-C. Lee, "Advanced nonlinear control of three-phase pwm rectifiers," *Electric Power Applications, IEE Proceedings* -, vol. 147, no. 5, pp. 361–366, Sep 2000.